Nanoscale
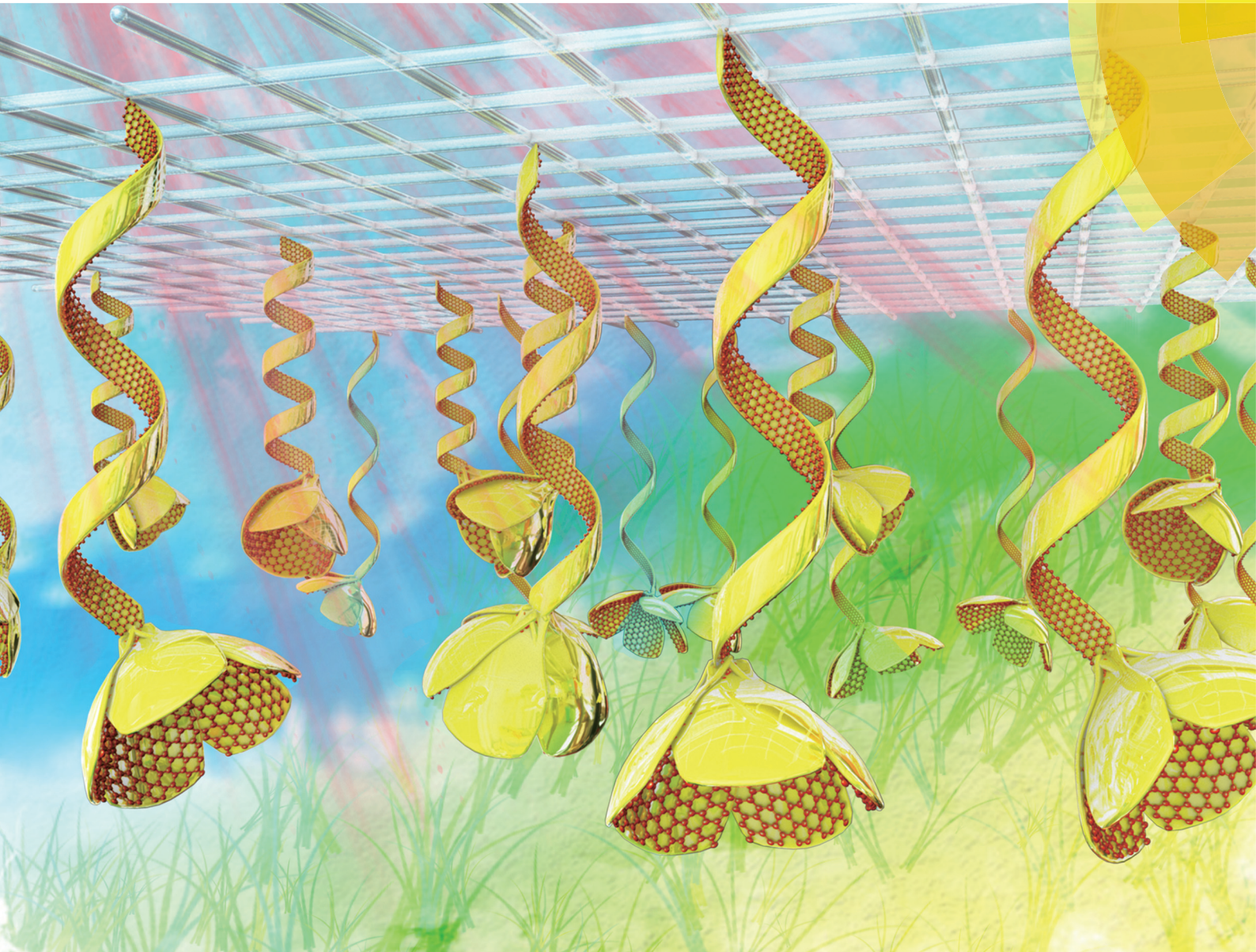
ROYAL SOCIETY
OF CHEMISTRY

PAPER
Luzhuo Chen, Wei Zhang *et al.*
Multi-responsive actuators based on a graphene oxide composite:
intelligent robot and bioinspired applications

NCNST

Check for updates

Multi-responsive actuators based on a graphene oxide composite: intelligent robot and bioinspired applications†

Luzhuo Chen, [ID] *‡[a,b] Mingcen Weng,‡[a,b] Peidi Zhou,[a,b] Lingling Zhang,[a,b] Zhigao Huang[a,b] and Wei Zhang [ID] *[a,b]

Carbon-based electrothermal or photothermal actuators have attracted intense attention recently. They can directly convert electrical or light energy into thermal energy and exhibit obvious deformations. However, if the actuation mechanism is only limited to thermal expansion, the deformation amplitude is difficult to increase further. Moreover, complex shape-deformation is still challenging. Although a few materials were reported to realize twisting or untwisting actuation by cutting the samples into strips along different orientations, each single strip could perform only one shape-deformation mode. In this work, we propose multi-responsive actuators based on a graphene oxide (GO) and biaxially oriented polypropylene (BOPP) composite, which are designed with different shapes (strip-shape and helical-shape). The strip-shape GO/BOPP actuator shows great bending actuations when driven by humidity (curvature of up to 3.1 cm^{-1}). Due to a developed dual-mode actuation mechanism, the actuator shows a bending curvature of 2.8 cm^{-1} when driven by near infrared (NIR) light. The great actuation outperforms most other carbon-based actuators. Then, an intelligent robot based on the GO/BOPP composite is fabricated, which can switch between the protection mode and weightlifting mode with different external stimuli. Inspired from plant tendrils, a bioinspired helical GO/BOPP actuator is further realized to show both twisting and untwisting actuations in a single actuator, fully mimicking the deformation of plant tendrils. Finally, a robot arm consisting of strip-shape and helical GO/BOPP actuators can grasp an object that is 2.9 times heavier than itself, demonstrating promising bioinspired applications.

Introduction

In recent years, carbon-based materials (using carbon nanotube or graphene) have triggered increasing research interest in both controllable fabrication and unique applications due to their fascinating properties.[1–5] Among them, carbon-based electrothermal or photothermal actuator materials can demonstrate obvious deformations under electrical or light stimulation.[6–14] They become one of the hot topics in the field of actuator materials and also push forward developments in many fields including robotics, artificial muscles and bio-

mimetic applications.[8,9,11,12,14] However, there are still some problems in this kind of material, which need to be solved urgently. For example, the actuation is mostly caused by the difference in the thermal expansion of a bilayer structure. If the actuation mechanism is only limited to thermal expansion, it is very difficult to further increase the deformation. Furthermore, complex deformation is difficult to realize through the simple strip-shape actuators. Although previous carbon-based material was reported to realize twisting or untwisting actuations by cutting the samples into strips along different orientations of carbon nanotubes, each single sample could perform only one shape-deformation mode (only twisting or only untwisting).[12] These issues together constrain the further development of this kind of material.

In this work, we propose an actuator material based on a graphene oxide (GO) and biaxially oriented polypropylene (BOPP) composite. The GO paper is prepared through a simple and fast vacuum filtration approach. The actuator can perform a large bending curvature of up to 3.1 cm^{-1} with humidity changes, which is attributed to the hygroexpansion effect of

aFujian Provincial Key Laboratory of Quantum Manipulation and New Energy Materials, College of Physics and Energy, Fujian Normal University, Fuzhou 350117, China. E-mail: chenluzhuo@163.com, wzhang721@163.com
bFujian Provincial Collaborative Innovation Center for Optoelectronic Semiconductors and Efficient Devices, Xiamen 361005, China
†Electronic supplementary information (ESI) available. See DOI: 10.1039/c7nr01913k
‡These authors contributed equally.

GO. It is also able to show a bending curvature of 2.8 cm^{-1} when driven by near infrared (NIR) light, which results from a dual-mode actuation mechanism. One mechanism is a great mismatch in the coefficient of thermal expansion (CTE) between GO and BOPP. The other is the thermohydration effect of GO. Then, an intelligent robot based on the GO/BOPP composite is fabricated. The robot can switch between the protection mode and weightlifting mode with different external stimuli. Furthermore, a helical GO/BOPP actuator is designed with inspiration from plant tendrils. Both twisting and untwisting actuations are realized in a single actuator, which fully mimics the deformation of plant tendrils and shows diversiform shape-deformations. The twisting/untwisting actuations can be transformed to each other when responding to different stimuli (NIR light and humidity). Finally, a robot arm based on one helical GO/BOPP actuator and four strip-shape GO/BOPP actuators is further constructed, which can untwist/open with increase in humidity and twist/close with NIR light irradiation. These applications show that the new designed actuator material has great potential in artificial muscles, robotics, bioinspired applications, and so on.

Results and discussion

Design of the GO/BOPP bilayer structure

GO is a layered material consisting of hydrophilic oxygenated graphene sheets bearing oxygen functional groups on their basal planes and edges. Free-standing GO papers have been fabricated by vacuum filtration for many years. The fabricated GO papers are flexible, lightweight (density of 1.8 g cm^{-3}) and high-strength (Young's modulus of ~32 GPa).[15] GO is usually served as a precursor for cost-effective and large-scale production of graphene-based materials with applications in field-effect transistors, sensors, transparent conductive films and clean energy devices.[16,17] GO is also a promising material for smart actuators.[18–20] However, to the best of our knowledge, multi-responsive actuator materials based on GO and polymers are still rare. In the meantime, polypropylene (PP) and BOPP have been used for actuators in recent years.[9,11,21–23] In this work, the reasons of selecting the GO/BOPP bilayer structure to fabricate high-performance actuator materials are as follows.

First, there are two mechanisms responsible for dimensional changes of a layer in response to heat or humidity: thermal expansion and hygroscopic expansion.[21] To maximize the actuation performance of a bilayer actuator, a possible solution is that one layer contracts while the other layer expands when heated. Therefore, one layer should have a small CTE and a large coefficient of hygroscopic expansion (CHE), while the other layer should have a large CTE and a small CHE. The properties of commonly used materials in flexible electronics are listed in Table S1 (ESI†). GO is different from most materials with positive CTEs. It apparently shows an obvious negative thermal expansion when heated.[15,24] In 2012, Kotov *et al.* revealed that the negative thermal expansion

of GO is in fact a pseudonegative thermal expansion, which is due to thermohydration effects. The intrinsic CTE of GO was found to be close-to-zero (0.85 ppm K^{-1}).[24] In addition, GO has a large CHE (2.7–9 × 10^{-2} %RH^{-1}).[25] After GO is selected as one layer of the bilayer actuator, another complementary material is needed to be the other layer of the bilayer actuator. As mentioned above, the complementary layer should have a CTE value that is large enough in contrast to that of the GO layer. Meanwhile, it should also have a small CHE as far as possible. As shown in Table S1,† BOPP has the second largest CTE value (up to 137 ppm K^{-1})[21] and the extremely low CHE value (moisture absorbance <0.03%).[23] In addition, although polydimethylsiloxane (PDMS) shows the largest CTE and a nearly undetectable CHE value, the relative long time for curing in the fabrication process excludes it from this work.

Second, motion is also an important factor for the actuator design and applications, which is greatly affected by the actuator configuration. Traditional actuator configuration is the uniform composite structure, which only leads to a simple motion such as expansion or contraction under external stimuli.[26] A bilayer structure could generate bending motion due to asymmetric deformation of two layers. We have proven that the bilayer structure is efficient in designing powerful and high-performance actuators in previous studies.[9,11,21] Moreover, more complicated motion such as twisting/untwisting and biomimetic walking can be achieved through proper design of the bilayer structure.[9,12]

Hence, we select GO and BOPP to fabricate a bilayer actuator.

Fabrication and characterization of the GO/BOPP actuator

The fabrication of the GO/BOPP bilayer structure is schematically illustrated in Fig. 1a. The fabrication process is simple, convenient and fast. First, vacuum filtration of colloidal dispersions of GO sheets through a membrane filter was conducted. After being dried, a piece of free-standing GO paper was obtained (see the Experimental section for details). As shown in Fig. 1b, GO paper is uniform with a thickness of ~30 μm. The fracture edges of GO paper are also imaged *via* a scanning electron microscope (SEM) (Fig. S1, ESI†), which shows well-packed layers through the cross-section of the GO paper. Second, a BOPP film was attached to the GO paper. The BOPP film is coated with acrylic ester and the total thickness is 40 μm. The acrylic ester is pressure sensitive adhesive with a thickness of ~15 μm (Fig. S2, ESI†). Finally, the GO/BOPP bilayer film was cut into a strip-shape with dimensions of 15 mm × 2 mm (length × width) to form an actuator. The optical photo of the GO/BOPP actuator is shown in Fig. 1c. The prepared GO/BOPP actuator is flexible (Fig. S3, ESI†) due to the excellent flexibility of the GO paper and BOPP film. Fig. 1d clearly demonstrates the layered structure of the GO/BOPP actuator. BOPP and GO layers are bonded to each other with the help of acrylic ester under pressure. Hence, the layers in the actuator are combined together tightly without delamination. As shown in a cross-sectional SEM image with higher magnification of the GO/BOPP actuator (Fig. S4, ESI†), the
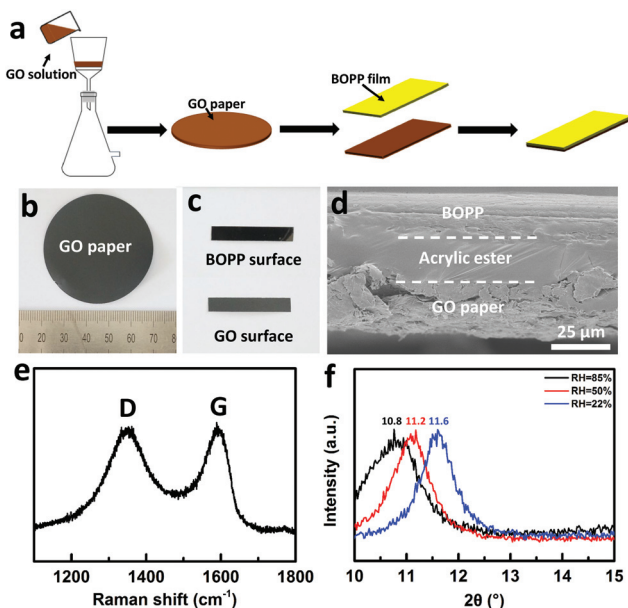
Fig. 1 Characteristics of the GO/BOPP actuator. (a) Schematic illustration of the fabrication process of the GO/BOPP actuator. (b) Optical photo of GO paper. (c) Optical photo of two surfaces of the GO/BOPP actuator. (d) Cross-sectional SEM image of the GO/BOPP actuator. (e) Raman spectrum of the GO paper. (f) XRD pattern of GO paper at different RHs (22%, 50% and 85%).

acrylic ester is tightly combined with GO paper. In a word, the entire fabrication process is simple and fast.

Furthermore, the Raman spectrum, X-ray diffraction (XRD) pattern and Fourier Transform Infrared (FT-IR) spectrum were collected for the characterization of GO paper. First, the Raman spectrum of GO paper is shown in Fig. 1e. There are two peaks: D-band (I_D) around 1352 cm^{-1} and G-band (I_G) around 1588 cm^{-1}. The G-band is related to graphitic carbon and the D-band is associated with the structural defects or partially disordered structures of graphitic domains. The FT-IR spectrum of GO paper is shown in Fig. S5 (ESI†). It confirms that there are many oxygen functional groups, which make the GO paper hygroscopic. Last, the XRD pattern of GO paper at an RH of 50% is shown in Fig. 1f (red line). XRD is used to measure the interlayer spacing of GO paper. The peak in the XRD pattern is around 11.2°, which corresponds to an interlayer spacing of 0.79 nm. From previous studies, this measured value can be attributed to an approximately one-molecule-thick layer of water between the GO sheets.[15]

Humidity-driven actuation of the GO/BOPP actuator

The GO/BOPP composite film is flexible (Fig. S3, ESI†), so it can be used for further arbitrary shape-deformation, which will benefit the applications in flexible actuating devices. There are numerous oxygen-containing groups on the surface of the GO, which makes it highly sensitive to humidity changes. The fast and reversible expansion/contraction of GO layers is evidenced through the adsorption and desorption of water molecules.[25,27] On the contrary, the BOPP film is inert to

water molecules.[21] Therefore, the GO/BOPP composite film should perform as a humidity-driven actuator.

In order to quantitatively investigate the actuation of the GO/BOPP actuator when driven by humidity, a transparent humidity control chamber was made to monitor the actuation as reported previously.[21] A 15 mm long actuator was firstly fabricated at an RH of 50%. Then it was suspended with a flat state. The top fixed end of the actuator (5 mm) was fixed to a glass substrate. When the GO/BOPP actuator was exposed to dry air (RH = 20%), a bending actuation to the GO side occurred (Fig. 2a). The curvature of the actuator was 2.5 cm^{-1} (the calculation of curvature is shown in Note S1 and Fig. S6, ESI†). When the RH returned to 50%, the actuator recovered to the initial flat state. Further increase of the RH would lead to the deformation of the GO/BOPP actuator to the BOPP side (Fig. 2c). The curvature was up to 3.1 cm^{-1}, which is due to the expansion of the GO layers caused by absorption of water molecules. Therefore, the actuator shows a bidirectional bending. When demonstrating the bidirectional bending in one figure, the curvature of the actuator bending to the GO side is defined as a positive curvature while that of bending to the BOPP side is defined as a negative curvature. The influence
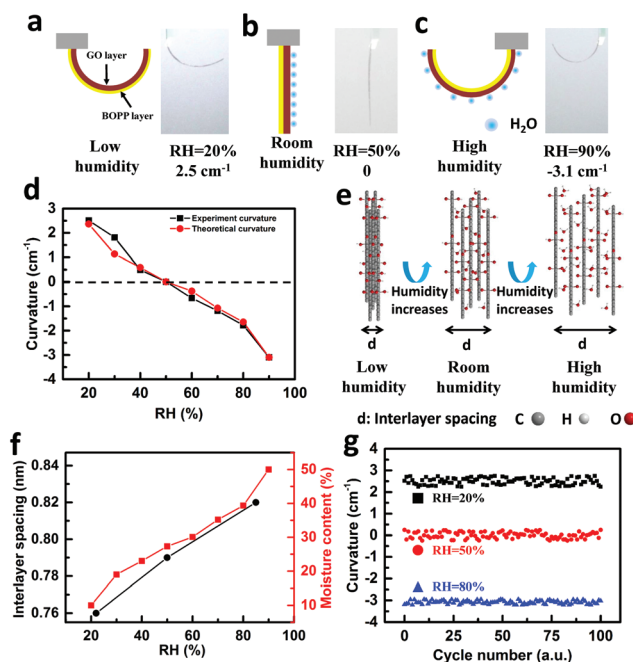

Fig. 2 GO/BOPP actuator responding to humidity. (a) Schematic illustration and optical photo of the GO/BOPP actuator at a low RH of 20%. (b) Schematic illustration and optical photo of the GO/BOPP actuator at room RH of 50%. (c) Schematic illustration and optical photo of the GO/BOPP actuator at a high RH of 90%. (d) Experiment curvature and theoretical curvature as a function of RH. (e) Schematic illustration of the interlayer spacing changes with the RH increases. (f) Interlayer spacing and moisture content as a function of RH. (g) Repeatability test of the GO/BOPP actuator undergoing repeated RH changes from 20% to 80%. The GO/BOPP actuator was fabricated at an RH of 50%. The dimensions of the GO/BOPP actuator were 15 mm × 2 mm × 65 μm (length × width × thickness).

of the RH on the bending curvature is presented in Fig. 2d (black line). The curvature of the GO/BOPP actuator changed from 2.5 cm^{-1} to 0, when the RH increased from 20% to 50%. Then it changed from 0 to 3.1 cm^{-1} with bending toward the other side, when the RH further increased from 50% to 90%. The related optical photos are shown in Fig. S7 (ESI).† The bending velocities of the GO/BOPP actuator with different RHs are also calculated, as shown in Fig. S8 (ESI).† When the RH was up to 90%, the actuator showed a bending actuation to the BOPP side with a maximum bending velocity of 0.052 cm^{-1} s^{-1}.

The humidity-driven mechanism can be explained by the hygroexpansion effect of GO. During the absorption stage, water molecules percolate to the hydrophilic regions of GO and increase the interlayer spacing of GO sheets (schematically shown in Fig. 2e). The saturation of these hydrophilic regions with water molecules causes GO sheets to slide apart from each other, resulting in the elongation of the GO paper. Therefore, the GO/BOPP actuator has bending motion with humidity changes. To confirm the mechanism of this moisture-responsive property, the interlayer spacing of GO sheets at different RHs was also measured by XRD (Fig. 1f). As shown in Fig. 1f, GO paper shows a diffraction peak at 11.2° at room humidity (RH of 50%), which corresponds to an interlayer spacing of 0.79 nm. However, when the RH decreases to 22%, the diffraction peak moves to 11.6° (Fig. 1f, blue line), indicating that the interlayer spacing decreases to 0.76 nm. When the RH increases to 85%, the diffraction peak moves to 10.8° (Fig. 1f, black line), indicating that the interlayer spacing increases to 0.82 nm. These results are in accordance with previous studies and confirm the humidity-driven mechanism.[20] Last, 100 cycles of repeated humidity alteration between 20% and 80% were conducted. The actuation performance remained stable (Fig. 2g). The result indicates the highly reliable actuation behavior of the GO/BOPP actuator.

To further understand the humidity-driven mechanism of the GO/BOPP actuator, a mechanical model is developed to simulate the curvature of the GO/BOPP actuator (Fig. S9 and Note S2, ESI†). The humidity inducing bending curvature of the GO/BOPP actuator can be expressed as:

$$\frac{1}{\rho} \propto \beta_1 \Delta C_1 \quad (1)$$

where $1/\rho$ is the bending curvature of the GO/BOPP actuator, β_1 is the CHE of the GO layer and ΔC_1 is the change of the moisture content in the GO layer, respectively.

To better evaluate the bending curvature of the GO/BOPP actuator, the moisture contents in GO paper at different RHs were measured (Fig. 2f, red line). On the basis of this, the theoretical curvatures of the GO/BOPP actuator driven by humidity are calculated and are also presented in Fig. 2d (red line). The theoretical curvatures are in accordance with the experiment results. Moreover, the interlayer spacing of the GO sheets remains in step with the moisture content in the GO layer (Fig. 2f, black line), which further confirms our humidity-

driven mechanism that is attributed to the hygroexpansion of GO paper.

NIR light-driven actuation of the GO/BOPP actuator

Owing to the photothermal conversion effect, photothermal actuators can convert light energy into thermal energy. Then, the actuators show actuations due to the great mismatch in the CTEs of materials when heated. Recently, photothermal actuators have been widely studied.[10,12] GO can absorb NIR light (Fig. S10, ESI†) and is a high-efficiency photothermal-conversion material, which can act as a heating layer to raise the temperature of the GO/BOPP actuator.[28] Meanwhile, GO has a close-to-zero intrinsic CTE of 0.85 ppm K^{-1}, while BOPP has a large positive CTE of 137 ppm K^{-1}. There is a great CTE mismatch between BOPP and GO. Moreover, the striking flexibility and mechanical robustness of GO and BOPP make them ideal candidates for the fabrication of light-driven actuators.

First of all, the actuation performance of the GO/BOPP actuator responding to NIR light was studied. When the GO/BOPP actuator is irradiated by NIR light, the GO layer absorbs light energy and converts it to thermal energy, leading to a bending motion of the GO/BOPP actuator. Similar to the humidity-driven test, the 15 mm long GO/BOPP actuator was fabricated at an RH of 50%, as shown in Fig. 3a. When NIR light irradiation (300 mW cm^{-2}) was on the BOPP side, the GO/BOPP actuator bent to the GO side within 10 s. The bending curvature was up to 2.8 cm^{-1}, demonstrating a large and fast photothermal actuation, as shown in Fig. 3b.
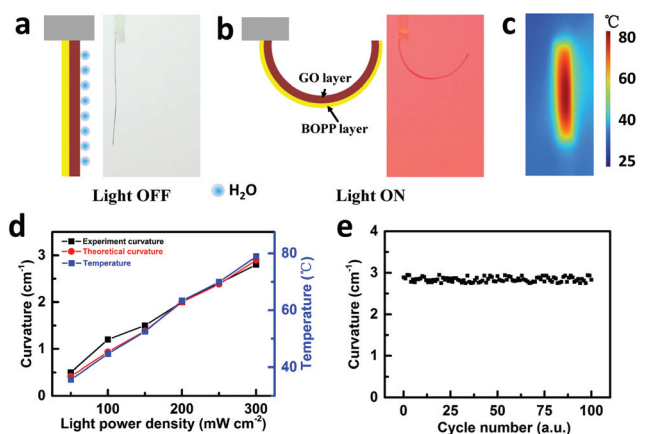

Fig. 3 GO/BOPP actuator responding to NIR light. (a) Schematic illustration and optical photo of the GO/BOPP actuator without NIR light. (b) Schematic illustration and optical photo of the GO/BOPP actuator with NIR light irradiation (300 mW cm^{-2}) for 10 s. (c) Infrared thermal image of the GO/BOPP actuator with NIR light irradiation (300 mW cm^{-2}) for 10 s. The actuator was fixed on a substrate without actuation. (d) Experiment curvature, theoretical curvature and temperature as a function of light power density. (e) Repeatability test of the GO/BOPP actuator undergoing repeated NIR light irradiation (300 mW cm^{-2}). The GO/BOPP actuator was fabricated at an RH of 50%. The experiment was conducted at an RH of 50%. The dimensions of the GO/BOPP actuator were 15 mm × 2 mm × 65 μm (length × width × thickness).

Furthermore, the GO/BOPP actuator was fixed on a glass substrate to investigate the temperature distribution of the actuator by an infrared thermal camera. After the actuator was irradiated by NIR light (300 mW cm^{-2}) for 10 s, the whole actuator showed a uniform temperature distribution at high temperature (~78.9 °C). The infrared thermal image of the GO/BOPP actuator is shown in Fig. 3c. Fig. 3d clearly shows the curvature and temperature of the actuator with different light power densities. When the GO/BOPP actuator was irradiated by low power NIR light (50 mW cm^{-2}) for 10 s, it showed a bending curvature of 0.5 cm^{-1} and the temperature was only 35.7 °C. The curvature increased to 2.8 cm^{-1} and the temperature was as high as 78.9 °C, when the actuator was irradiated by high power NIR light (300 mW cm^{-2}). The corresponding optical photos of the GO/BOPP actuator are shown in Fig. S11 (ESI).† Obviously, more NIR light is converted into thermal energy by the GO layer with a larger light power density, resulting in a higher temperature. It is obvious that different curvatures can be obtained by using different light power densities. Therefore, Fig. 3d also shows the controllability of the actuator. The bending velocities of the GO/BOPP actuator with different light power densities are also calculated, as shown in Fig. S12 (ESI).† When the light power density was up to 300 mW cm^{-2}, the actuator showed a bending actuation to the GO side with a maximum bending velocity of 0.28 cm^{-1} s^{-1}, which is about 5 times faster than the maximum humidity-driven bending velocity. With NIR light irradiation, the light to thermal conversion efficiency of GO is calculated to be 76.5%. The calculation method was described in our previous study.[21] Finally, the repeatability of the NIR light-driven actuation of the actuator was also tested. As shown in Fig. 3e, the actuation performance had no significant degradation after 100 cycles, which indicates good reliability and stability. The cross-sectional SEM image of the actuator after the repeatability test is also shown in Fig. S13 (ESI).† It shows that the BOPP layer and GO layer are still tightly combined after the repeatability test.

The light-driven actuation mechanism of the GO/BOPP actuator is as follows. Two mechanisms together result in the great bending performance of the GO/BOPP actuator. First, GO has the hygroexpansion effect, which exhibits as the thermohydration effect when GO is heated. When the GO/BOPP actuator is irradiated by NIR light, the graphite layer absorbs light energy. Then, the absorbed light energy is quickly converted into thermal energy, resulting in a temperature increase of the GO layer. Correspondingly, the heating process will induce desorption of water molecules between the GO sheets. The decrease of interlayer spacing of the GO sheets leads to the contraction of the GO layer. Second, there is a great CTE mismatch between GO and BOPP. As the thermohydration effect in GO is considered, the intrinsic CTE of GO (0.85 ppm K^{-1}) should be used, preventing a double counting. Meanwhile, the BOPP has a large positive CTE (up to 137 ppm K^{-1}). As the BOPP layer and GO layer are tightly combined by acrylic ester, the heat is effectively transported from the GO layer to the BOPP layer. Therefore, the temperature rise of the actuator leads to the larger thermal expansion of the BOPP layer, com-

pared to that of the GO layer, which finally results in the actuator bending to the GO layer side. Due to such a dual-mode actuation mechanism, the GO/BOPP actuator shows great bending performance when driven by NIR light. Fig. S14 (ESI)† shows that the curvature increased quickly with the increase of temperature during NIR light irradiation. The variation trends of curvature and temperature were nearly synchronously. However, their variation trends are different after the NIR light is turned off. The descending speed of temperature is much faster than that of curvature. The similar asynchronous phenomena and reasons have been reported in previous studies,[21,24] which also prove the dual-mode actuation mechanism. The actuation is attributed to the thermal expansion differences of GO and BOPP and the thermohydration effect of GO.

Moreover, the mechanical model was also used to analyze the bending performance of the actuator driven by NIR light (Fig. S9 and Note S3, ESI†). Due to the dual-mode actuation mechanism, the bending curvature of the GO/BOPP actuator can be expressed as:

$$\frac{1}{\rho} \propto \alpha_2 \Delta T - \alpha_1 \Delta T - \beta_1 \Delta C_1 \qquad (2)$$

where α_1 and α_2 are the CTE of GO and BOPP, respectively, ΔT is the temperature change, β_1 is the CHE of GO and ΔC_1 is the change of the moisture content in the GO. To more accurately evaluate the bending curvature of the actuators, the moisture contents of the GO paper at different temperatures were also measured. The moisture content linearly declines as the temperature increases (Fig. S15a, ESI†). As the relationship between the moisture content of GO paper and the temperature change is given, the curvature value can be predicted as a function of the light power density (Fig. S15b, ESI†). The calculated curvatures are also shown in Fig. 3d, which are in accordance with the experiment curvatures. The curvatures of the actuator considering only one actuation mechanism (e.g. contraction of the GO layer, or thermal expansion of the BOPP layer and GO layer) are also calculated for comparison (Fig. S15b, ESI†). The calculated curvatures considering only one actuation mechanism are both much smaller than the curvature considering the dual-mode actuation mechanism. Our theoretical model also indicates that 65% of the bending actuation is attributed to the contraction of the GO layer, while 35% of the actuation is attributed to the thermal expansion differences of the BOPP and GO layers. Such a result also proves the indispensability of both GO and BOPP in our actuator.

The blocking force of the light-driven actuator was also measured with a strip-shape GO/BOPP actuator (at the tip of the actuator). The detected maximum blocking force is 4.1 mN (410 mg) as shown in Fig. S16 (ESI†). A noteworthy point is that force density (blocking force divided by the weight of the actuator) is a key factor for the effective force generation of an actuator. In the GO/BOPP actuator, the force density is about 55, which means that the force is 55 times higher than its own weight (7.4 mg), demonstrating the potential mechanical application of GO/BOPP actuators.

Finally, we also studied the influence of the GO layer thickness on the actuation performance. Experiment results showed that the optimal thickness of the GO layer to obtain a large curvature is in the range of 25.5 μm to 44.3 μm (see Note S4 and Fig. S17 in the ESI† for details). Hence, it is appropriate to select the thickness of the GO layer as 30 μm in this study, which is also used in the following applications.

Intelligent robot based on the GO/BOPP actuator

To extend the utilization of the multi-responsive characteristic of the GO/BOPP actuator, an intelligent robot was designed. Fig. 4a and b give the schematic illustrations of the intelligent robot configuration. The BOPP films were attached to both sides of GO paper (see the Experimental section for details). The robot was flat in its initial state. An object was placed in the middle of the robot (Fig. 4b and c). When the humidity increased, four feet of the robot gradually bent upwards to form a box-shape configuration, protecting and hiding the inside object (Fig. 4d). When NIR light (100 mW cm^{-2}) was turned on, the folded robot gradually opened (Fig. 4e). Finally, the four feet of the robot even bent downwards, lifting up the object with a distance of 10 mm. Hence, the intelligent robot is able to switch between the protection mode and the weightlifting mode with different external stimuli.

Bioinspired helical GO/BOPP actuator and its application

Helical twisting is a more complicated 3D shape-deformation, which is more challenging than bending deformation. Inspired from plant tendrils, a bioinspired helical actuator based on the GO/BOPP composite was assembled to demonstrate the capability of varied and tunable shape-deformations. A strip-shape GO/BOPP actuator (60 mm × 5 mm) was wound around a glass rod with the BOPP film on the outer side. After a heat treatment at 100 °C in a vacuum oven for 12 h, a helical actuator was well-prepared. The fabricated helical actuator was then placed at an RH of 50% for further use (middle panel of Fig. 5a).

Upon humidity increase, the helical actuator performs an untwisting actuation accompanied by a length elongation. The maximum elongation rate of the helical actuator was up to ~70% with an increase in humidity for 25 s (left panel of Fig. 5a). When irradiated by NIR light, the helical actuator exhibited a rapid twisting actuation accompanied by a length contraction. When irradiated by NIR light (300 mW cm^{-2}) for 15 s, the maximum contraction rate of the helical actuator was ~30% (right panel of Fig. 5a). The rotation angle of untwisting actuation reaches ~990° with an untwisting rotation speed of 6.6 rotations per minute (rpm), while the rotation angle of twisting actuation reaches ~1710° with a twisting rotation speed of 19 rpm. The twisting and untwisting actuations were highly reversible, as shown in Fig. 5b. There was no obvious degradation after 100 cycles. Hence, the bioinspired helical actuator is multi-responsive, showing both twisting and untwisting actuations when driven by NIR light and humidity respectively (Movie S1, ESI†). Such twisting and untwisting actuations fully mimic the deformation of plant tendrils and have not been demonstrated in a single actuator in previous studies.
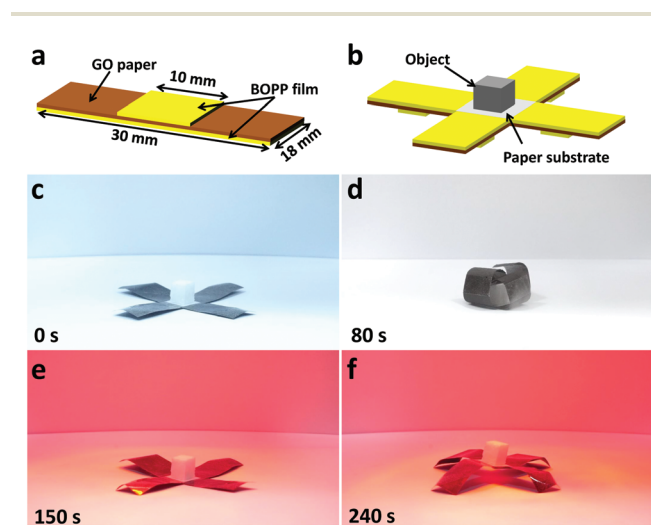

Fig. 4 (a) Schematic illustration of one foot of the intelligent robot. (b) Schematic illustration of the intelligent robot. (c) Optical photo showing the initial state of the intelligent robot. (d) Optical photo showing the protection mode of the intelligent robot responding to humidity. (e) Optical photo showing the intelligent robot responding to NIR light. (f) Optical photo showing the weightlifting mode of the intelligent robot responding to NIR light.
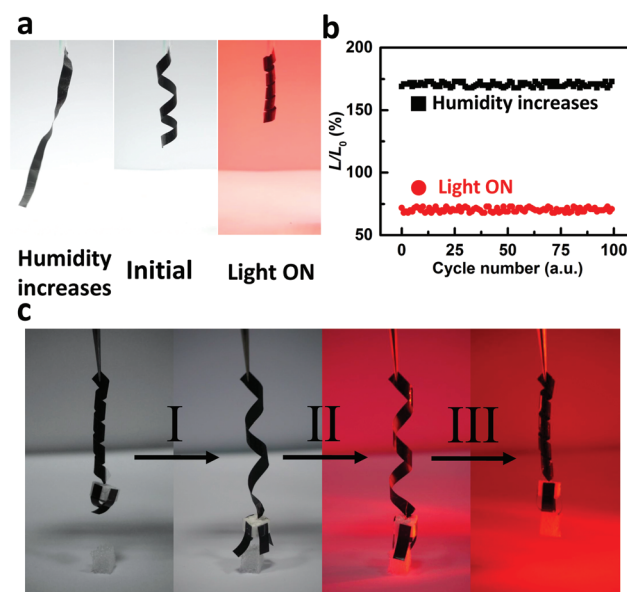

Fig. 5 (a) Optical photos of the helical GO/BOPP actuator: initial state (middle panel), deformation driven by humidity increase for 30 s (left panel) and NIR light irradiation (300 mW cm^{-2}) for 15 s (right panel). (b) Repeatability test of the twisting and untwisting actuations of the GO/BOPP helical actuator. L_0 is the initial length, L is the length which responds to the increase in humidity or NIR light irradiation. (c) Optical photos of a robot arm based on GO/BOPP actuators grasping/releasing an object.

Finally, we would like to leverage the excellent properties of the GO/BOPP actuator in bioinspired applications. A robot arm consisting of a helical GO/BOPP actuator and four strip-shape GO/BOPP actuators (40 mm × 5 mm) was fabricated. The helical actuator served as a telescopic arm and the four strip-shape actuators together served as a claw at the bottom of the arm. The robot arm can conduct grasping/releasing and elongation/contraction performances with external stimuli (NIR light irradiation or humidity increase). The robot arm can carry an object which is 2.9 times heavier than itself. The movement of manipulating an object is demonstrated in Fig. 5c and Movie S2 (ESI†). When humidity increased, the robot arm untwisted and the claw opened in Step I. Then, when NIR light was irradiated on the claw, the claw grasped the object in Step II. At last, when the whole robot arm was irradiated by NIR light, the object was lifted up in Step III. The robot arm shows that the GO/BOPP actuators have great potential in artificial muscles, intelligent robots and bioinspired applications.

Conclusions

In summary, multi-responsive GO/BOPP actuators are fabricated through a simple, scalable and fast fabrication approach. The strip-shape GO/BOPP actuator shows great bending performance with NIR light or humidity changes. The high CHE, the close-to-zero intrinsic CTE of GO paper and the large positive CTE of the BOPP film are all attributed to the high-performance of the actuator. The attained actuation performance of the GO/BOPP actuators outperforms many recently reported actuators based on BOPP (PP) or GO (Table S2, ESI†). An intelligent robot based on the GO/BOPP composite is further fabricated, showing protection mode and weightlifting mode with different external stimuli. Finally, a prototype of the robot arm consisting of one bioinspired helical GO/BOPP actuator and four strip-shape GO/BOPP actuators is elaborately designed and constructed. It demonstrates twisting and untwisting actuations and promising bioinspired applications of the GO/BOPP composite. With further improvement, this new designed composite will not only provide a route to realize complex shape-deformations, but also build up a platform based on emerging multi-responsive actuator materials for the development of high-performance artificial muscles, bioinspired robotics, and so on.

Experimental section

Fabrication of GO paper

GO was purchased from Suzhou Tanfeng Graphene Science and Technology Co., Ltd China. GO paper was prepared by vacuum filtration of the GO aqueous solution (2.5 mg ml^{-1}, 20 ml) through a membrane filter (0.45 μm in pore size). Then it was followed by a drying process at room temperature for 6 hours. Finally, the GO paper was peeled off from the membrane for further use.

Fabrication of the GO/BOPP bilayer film

The GO paper with a thickness of 30 μm was prepared as described above. It was cut into a rectangular-shape with the dimensions of 40 mm × 10 mm (length × width) and spread on a flat glass. A commercial acrylic-ester-coated BOPP film was attached to the GO paper to form an actuator at an RH of 50%. The dimensions of the acrylic-ester-coated BOPP film were 40 mm × 18 mm × 40 μm (length × width × thickness). Finally, the GO/BOPP composite film was cut into a strip-shape with dimensions of 15 mm × 2 mm × 65 μm (length × width × thickness) to form an actuator for further test.

Fabrication of the intelligent robot

First, a BOPP film was attached to GO paper at an RH of 50% to form a GO/BOPP bilayer film. The dimensions were 30 mm × 18 mm (length × width). Second, another BOPP film with dimensions of 10 mm × 18 mm (length × width) was attached to the other surface of GO paper in the middle, so as to form one foot of the intelligent robot (Fig. 4a). Third, three feet of the intelligent robot were fabricated by repeating the above process. Finally, four feet (45 mg × 4) were connected to a paper substrate (80.5 mg) to form the intelligent robot.

Fabrication of the helical GO/BOPP actuator

First, a BOPP film was attached to GO paper at an RH of 50% to form a GO/BOPP bilayer film. The dimensions were 60 mm × 5 mm (length × width). The GO/BOPP bilayer film was wound on a glass rod (radius of 5 mm) with the BOPP film on the outer side. The helical actuator was prepared after a heat treatment at 100 °C in a vacuum oven for 12 h. The fabricated helical actuator was then placed at an RH of 50% for further use.

Humidity-driven test

When the actuator was placed in a humidity control chamber, a steady-state curvature was achieved within 60 s. The steady-state was confirmed by observing that the curvature of the actuator remained unchanged for another 60 s.

Light-driven test

The actuator was placed in the humidity control chamber. In order to keep the same initial flat state, the actuator was fabricated in the chamber at an RH of 50% for further use. The light-driven tests were carried out in the humidity control chamber.

Moisture contents of GO paper

First, thermal-induced moisture loss of GO paper was tested as follows. The weight of the GO paper was measured by using a precision balance (YOKEFA1004CS) at room temperature. The GO paper was then placed into an oven at different temperatures ranging from 30 °C to 100 °C. The GO paper was kept inside the oven for 1 min at each temperature. Then it was immediately weighed by the precision balance. The GO paper is assumed to be completely dry at 100 °C. The moisture

concentration was calculated as $C_T = (M_T - M_{Dry})/M_{Dry}$, where M_T is the weight of the GO paper at different temperatures and M_{Dry} is the weight of GO paper at 100 °C. Second, the humidity-induced moisture change of GO paper was tested as follows. The GO paper was placed into a chamber under different RHs from 20% to 90% and was kept inside the chamber for 1 min. Then it was immediately weighed. The moisture concentration was calculated as $C_{RH} = (M_{RH} - M_{Dry})/M_{Dry}$, where M_{RH} is the weight of the GO paper at different RHs. The measuring method is consistent with a reported study.[23]

Blocking force measurement

An actuator (15 mm × 2 mm) was connected to a PDMS cube (10.78 mN, 1078 mg) as a preload. It was then placed on a precision balance with axial configurations. The generated forces of the actuator were measured as a function of the NIR light power densities (operating for 10 s). The measuring method is consistent with a reported study.[23]

Characterization and measurement

The SEM images were captured by a field-emission scanning electron microscope (Hitachi SU8010). The Raman spectra were recorded at room temperature by using a HORIBA JobinYvon Evolution Raman spectrometer with the 532 nm He–Ne laser line. The absorption spectra were recorded by using a UV/VIS/NIR spectrometer (PerkinElmer Lambda 950). The XRD pattern was measured by using an X-ray diffractometer (XRD, Rigaku MiniFlex II) with CuKα radiation (λ = 0.15405 nm). FT-IR spectra were recorded by using a FT-IR spectrometer (Nicolet IS50). The bending curvatures of the actuator, all optical images and videos were captured by a digital camera (SONY ILCE 6000). A NIR light source (Philips BR125) was used for light-driven actuation. The light power density was measured by using an IR Power Meter (Linshang LS122A). The temperature was recorded by using a laser sight infrared thermometer (Optris LS) with a temperature resolution of 0.1 °C. The temperature data were obtained from the GO surface of the actuator. The emissivity coefficient was set to be 0.95. The temperature of the BOPP surface was also measured and it was nearly the same as the temperature of the GO surface. An infrared thermal imager (Fluke Ti10) was used to characterize the thermal distribution of the actuator. The weights of samples were measured using by a precision balance (YOKEFA1004CS). The high RH (e.g., 90%) was supplied by a humidifier and monitored by a hygrometer, while the low RH was available by exposure to the ambient environment or obtained by a dehumidifier.

Notes and references

1 Y. Huang, J. Liang and Y. Chen, *J. Mater. Chem.*, 2012, **22**, 3671.
2 Y. Zhao, L. Song, Z. Zhang and L. Qu, *Energy Environ. Sci.*, 2013, **6**, 3520.
3 S. Wan, J. Peng, L. Jiang and Q. Cheng, *Adv. Mater.*, 2016, **28**, 7862.
4 Z. Li, Z. Liu, H. Sun and C. Gao, *Chem. Rev.*, 2015, **115**, 7046.
5 F. Béguin, V. Presser, A. Balducci and E. Frackowiak, *Adv. Mater.*, 2014, **26**, 2219.
6 L. Chen, C. Liu, K. Liu, C. Meng, C. Hu, J. Wang and S. Fan, *ACS Nano*, 2011, **5**, 1588.
7 X. Zhang, Z. Yu, C. Wang, D. Zarrouk, J. T. Seo, J. C. Cheng, A. D. Buchan, K. Takei, Y. Zhao, J. W. Ager, J. Zhang, M. Hettick, M. C. Hersam, A. P. Pisano, R. S. Fearing and A. Javey, *Nat. Commun.*, 2014, **5**, 2983.
8 Y. Hu, T. Lan, G. Wu, Z. Zhu and W. Chen, *Nanoscale*, 2014, **6**, 12703.
9 L. Chen, M. Weng, Z. Zhou, Y. Zhou, L. Zhang, J. Li, Z. Huang, W. Zhang, C. Liu and S. Fan, *ACS Nano*, 2015, **9**, 12189.
10 Y. Hu, Z. Li, T. Lan and W. Chen, *Adv. Mater.*, 2016, **28**, 10548.
11 L. Chen, M. Weng, W. Zhang, Z. Zhou, Y. Zhou, D. Xia, J. Li, Z. Huang, C. Liu and S. Fan, *Nanoscale*, 2016, **8**, 6877.
12 J. Deng, J. Li, P. Chen, X. Fang, X. Sun, Y. Jiang, W. Weng, B. Wang and H. Peng, *J. Am. Chem. Soc.*, 2016, **138**, 225.
13 W. Zhang, M. Weng, P. Zhou, L. Chen, Z. Huang, L. Zhang, C. Liu and S. Fan, *Carbon*, 2017, **116**, 625.
14 P. Xiao, N. Yi, T. Zhang, Y. Huang, H. Chang, Y. Yang, Y. Zhou and Y. Chen, *Adv. Sci.*, 2016, **3**, 1500438.
15 D. A. Dikin, S. Stankovich, E. J. Zimney, R. D. Piner, G. H. B. Dommett, G. Evmenenko, S. T. Nguyen and R. S. Ruoff, *Nature*, 2007, **448**, 457.
16 Y. Zhu, S. Murali, W. Cai, X. Li, J. W. Suk, J. R. Potts and R. S. Ruoff, *Adv. Mater.*, 2010, **22**, 3906.
17 L. Wen, F. Li and H. Cheng, *Adv. Mater.*, 2016, **28**, 4306.
18 Y. Jiang, C. Hu, H. Cheng, C. Li, T. Xu, Y. Zhao, H. Shao and L. Qu, *ACS Nano*, 2016, **10**, 4735.
19 D. Han, Y. Zhang, Y. Liu, Y. Liu, H. Jiang, B. Han, X. Fu, H. Ding, H. Xu and H. Sun, *Adv. Funct. Mater.*, 2015, **25**, 4548.
20 D. Han, Y. Zhang, H. Jiang, H. Xia, J. Feng, Q. Chen, H. Xu and H. Sun, *Adv. Mater.*, 2015, **27**, 332.
21 M. Weng, P. Zhou, L. Chen, L. Zhang, W. Zhang, Z. Huang, C. Liu and S. Fan, *Adv. Funct. Mater.*, 2016, **26**, 7244.
22 Y. Jin, B. Shin-Il Kim, W. Lee, C. Lee, H. Kim, K. Song, S. Jang and G. Kwak, *NPG Asia Mater.*, 2014, **6**, e137.
23 M. Amjadi and M. Sitti, *ACS Nano*, 2016, **10**, 10202.

24 J. Zhu, C. M. Andres, J. Xu, A. Ramamoorthy, T. Tsotsis and N. A. Kotov, *ACS Nano*, 2012, **6**, 8357.

25 H. Cheng, J. Liu, Y. Zhao, C. Hu, Z. Zhang, N. Chen, L. Jiang and L. Qu, *Angew. Chem., Int. Ed.*, 2013, **52**, 10482.

26 L. Z. Chen, C. H. Liu, C. H. Hu and S. S. Fan, *Appl. Phys. Lett.*, 2008, **75**, 263104.

27 S. Park, J. An, J. W. Suk and R. S. Ruoff, *Small*, 2010, **6**, 210.

28 M. Ji, N. Jiang, J. Chang and J. Sun, *Adv. Funct. Mater.*, 2014, **24**, 5412.